Analysis and Optimization of Grid Oscillators

Wayne A. Shiroma, *Member, IEEE*, and Zoya Basta Popović, *Member, IEEE*

***Abstract*— A method for assessing and optimizing the feedback level in a transistor-grid oscillator is presented. Based on the approximate large-signal S-parameters of the transistor, an equivalent circuit model for the grid is synthesized for maximum oscillator power. The resulting circuit serves as a convenient benchmark for determining the level of feedback for a given grid. Experimental results are presented for five different grid oscillators covering S through Ka bands. By varying the substrate thickness and metallization pattern of the grid, the feedback can be optimized in accordance with the theory. A grid with an asymmetric unit cell is shown to deliver almost 60% more effective radiated power (ERP) than a grid with a symmetric unit cell.**

***Index Terms*— Active arrays, millimeter-wave oscillators, millimeter-wave power dividers/combiners, quasi-optical arrays.**

I. Introduction

GRID oscillators are large-scale power combiners that have shown promise for realizing moderate to high-power millimeter-wave sources [1]–[3]. A grid oscillator is shown schematically in Fig. 1, where a metal grating is loaded with either two- or three-terminal solid-state devices. The grating is etched on a dielectric substrate and has a period much smaller than a free-space wavelength. The vertical leads of the grating serve as antennas, and the horizontal leads as dc bias lines. If properly designed, the bias lines do not affect the high-frequency performance of the active grid, as the radiated electric field is vertically polarized. A mirror is placed behind the grid to provide the positive feedback necessary for oscillation. A partially transparent reflector is sometimes placed in front of the grid. This configuration is analogous to a Fabry–Perot cavity laser, where the active grid serves as the gain medium.

When dc bias is applied, an oscillation is triggered by transients or noise, and each device oscillates at a different frequency. An incoherent wave radiates from the grid, reflects off the mirrors, and injection-locks the oscillating devices. At the onset of oscillation, different cavity modes compete, as in a laser. Since most grid oscillators use low-Q unstable Fabry–Perot resonators, the mode with the lowest diffraction loss most likely dominates [3]. After a few round trips, the higher order modes lose most of their power to diffraction, resulting in a single-frequency self-locked coherent oscillation.

Manuscript received March 25, 1997; revised August 4, 1997. This work was supported in part by the U.S. Army Research Office under Contract DAAL03-92-G-0265 and the AASERT Program, and in part by the National Science Foundation through a Presidential Faculty Fellow Award.

W. A. Shiroma is with the Department of Electrical Engineering, University of Hawaii at Manoa, Honolulu, HI 96822 USA.

Z. B. Popović is with the Department of Electrical and Computer Engineering, University of Colorado, Boulder, CO 80309 USA.

Publisher Item Identifier S 0018-9480(97)08335-X.

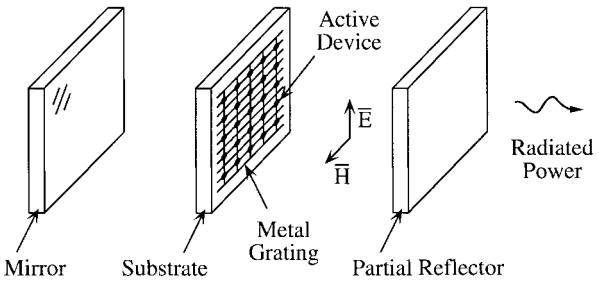

Fig. 1. A grid oscillator, consisting of an active-device array placed within a Fabry–Perot cavity.

Designing a grid oscillator requires that the steady-state oscillation condition [4] be met. In addition, for a power-grid design, the load resistance must be optimized and the feedback level adjusted so that the device operates at maximum power-added efficiency [5]. To meet all of these constraints simultaneously at the desired oscillation frequency, the grid dimensions, substrate parameters, metallization pattern, and mirror positions must be adjusted iteratively. Even with the aid of equivalent circuit models, this process can be quite tedious and time consuming.

This paper describes a synthesis procedure that not only incorporates the oscillation condition, but also optimizes the feedback level and load impedance of a grid oscillator. Section II begins by describing how the circular function [6] accurately models grid oscillators. It also discusses how a grid can be reduced to an equivalent two-port embedding circuit that can be used to analyze a grid from the standpoint of negative resistance. Section III presents a method for optimizing this embedding circuit to maximize oscillator power. This optimum circuit, together with its associated circular function, is used as a benchmark for assessing and improving the performance of several experimental grids in Sections IV and V.

II. Grid-Oscillator Analysis

A. Circular-Function Analysis

Grid oscillators are most often analyzed using the unit-cell approximation [1], in which it is assumed that the grid is infinite in extent and that the devices oscillate at the same frequency and phase. As shown in Fig. 2(a), the unit cell can be separated into two components: the embedding circuit (consisting of the metal grating, dielectric substrate, mirror, and free space), which can be characterized using approximate [1] or full-wave [7] methods, and the active device, which can be characterized using linear S-parameters or a nonlinear circuit model. For a transistor array, both the embedding circuit

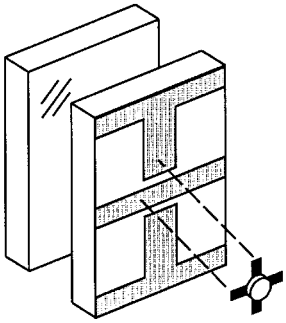

(a)

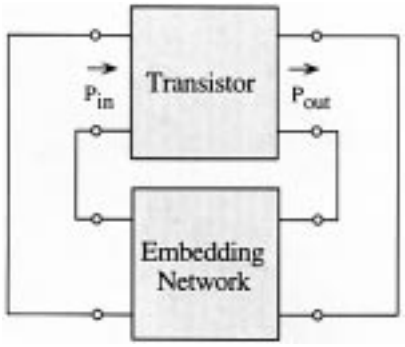

(b)

Fig. 2. (a) Unit cell of a grid oscillator with the transistor and passive grid separated. (b) Feedback-oscillator model consisting of the embedding network and the transistor model. $P_{\rm in}$ and $P_{\rm out}$ represent the input and output power of the transistor, respectively. The power dissipated in the embedding network $P_{\rm out} - P_{\rm in}$ is the actual power radiated by the grid oscillator.

and device model can be represented as two-port networks, where the ports represent, for example, the gate–source and drain–source ports of a MESFET. A grid oscillator can then be viewed as a quasi-optical implementation of a two-port feedback oscillator [see Fig. 2(b)].

The generalized steady-state oscillation condition [4] of an n-port feedback oscillator is

$$\det(\mathbf{SS'} - \mathbf{I}) = \mathbf{0} \tag{1}$$

where $\mathbf{S}$ and $\mathbf{S'}$ are the n-port scattering matrices of the device and embedding networks, respectively.

For $n = 2$, as in Fig. 2(b), (1) reduces to

$$S_{11}S'_{11} + S_{12}S'_{21} + S_{21}S'_{12} + S_{22}S'_{22} - |\mathbf{S}||\mathbf{S'}| = 1 \tag{2}$$

where

$$|\mathbf{S}| = S_{11}S_{22} - S_{12}S_{21}$$

and

$$|\mathbf{S'}| = S'_{11}S'_{22} - S'_{12}S'_{21}.$$

A circuit simulator can be used to analyze this closed-loop circuit by breaking the loop at some point and inserting a probe (Fig. 3). The simulator then determines the loop gain b''_1/a''_1. If a standard circulator is used as the probe, the signal-flow graph in Fig. 4 results. Applying Mason's rule [8] to this graph results in the following expression for the loop gain, or

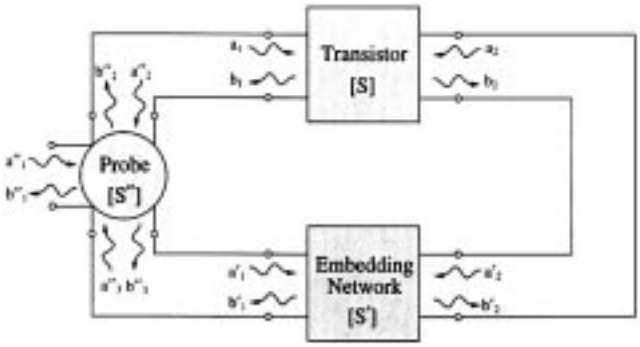

Fig. 3. Feedback oscillator with a circuit probe inserted into the feedback path.

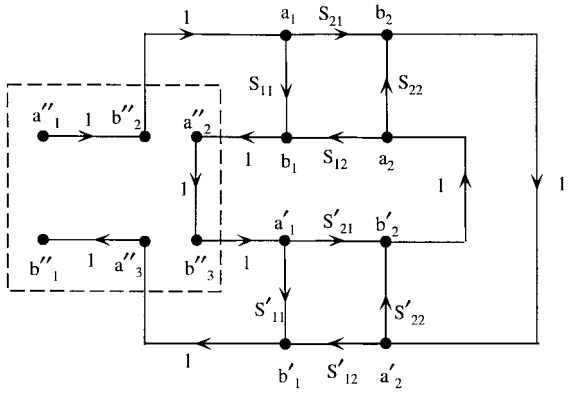

Fig. 4. Signal-flow graph for the feedback oscillator with a circulator probe. The dashed box encloses the signal-flow graph for the circulator.

circular function, as it is referred to in [6]:

$$C = \frac{b''_1}{a''_1} = \frac{S_{11}S'_{11} + S_{21}S'_{12} - |\mathbf{S}||\mathbf{S'}|}{1 - S_{12}S'_{21} - S_{22}S'_{22}}. \tag{3}$$

Note that when $C = 1\angle 0°$, (3) is equivalent to the steady-state oscillation condition (2).

If (3) is evaluated using the transistor's small-signal S-parameters, oscillation start-up requires that $|C| > 1$. To reach steady state, gain compression causes the transistor S-parameters to saturate until the condition $C = 1\angle 0°$ is satisfied at the oscillation frequency.

Fig. 5 illustrates the circular-function analysis of two grid oscillators with identical unit cells, but with different substrate and mirror characteristics. Fig. 5(a) shows the circular function for a transistor-loaded grid in free space, with no dielectric substrate or mirror. Since the magnitude of the circular function is less than one, no oscillation is possible. However, when the grid is backed by a 6.35-mm-thick substrate with $\epsilon_r = 10.2$, two modes are predicted at 2.8 and 6.5 GHz [see Fig. 5(b)]. This agrees with measured oscillation modes at 2.7 and 6.4 GHz (Fig. 6).

Another example is a monolithic 100-element pseudomorphic high electron-mobility transistor (100-pHEMT) grid oscillator that was designed by the University of Colorado, fabricated by Honeywell, and tested by TLC Precision Wafer Technology, Inc. The grid is fabricated on a 100-μm-thick GaAs wafer and placed on a 254-μm-thick alumina substrate

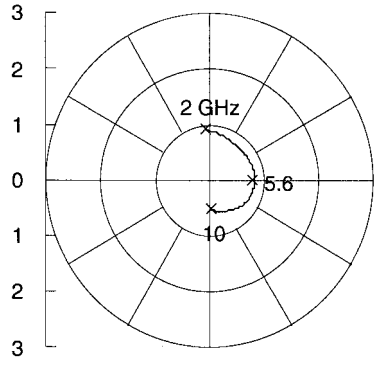

(a)

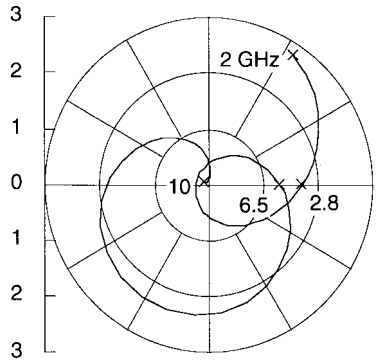

(b)

Fig. 5. Circular functions for a transistor-loaded grid (a) in free space, with no substrate or mirror, and (b) backed by a thick high-permittivity substrate and mirror. The active device is an HP-Avantek ATF-26836 general-purpose MESFET. Small-signal S-parameters (for $V_{\rm ds} = 3$ V, $I_{\rm ds} = 10$ mA) supplied by the manufacturer are used in the simulation.

metallized on one side. The unit cell is 300-μm square with 30-μm-wide bias lines and radiating leads. The circular function predicts an oscillation near 31.2 GHz (Fig. 7). The measured oscillation frequency is 31.1 GHz [9].

B. Negative-Resistance Grid Model

Since the passive embedding network for the grid is reciprocal, it can be represented as a lumped equivalent circuit, as shown in Fig. 8(a), where Y_{ij} are the associated two-port Y-parameters. For a typical unit cell [e.g., Fig. 2(a)], this equivalent circuit takes the form shown in Fig. 8(b). The capacitors C_1 and C_2 model the gate–source and drain–source gaps of the grid, respectively. The inductor and resistor model the lead inductance, substrate thickness, mirror position, and radiation into free space. Connecting the equivalent circuit to the transistor results in the model shown in Fig. 9(a). If the resistor is removed, an equivalent one-port negative-resistance model of the grid oscillator is obtained [see Fig. 9(b)]. Oscillation start-up requires that the absolute value of this negative resistance be greater than the load resistance. Using this model, we can reexamine the cases described earlier.

Fig. 10(a) and (b) shows the negative-resistance models whose circular functions were plotted in Fig. 5(a) and (b), respectively. In Fig. 10(a), since the magnitude of the negative resistance of the embedded device is less than the load resistance, no oscillation is possible. In Fig. 10(b), two

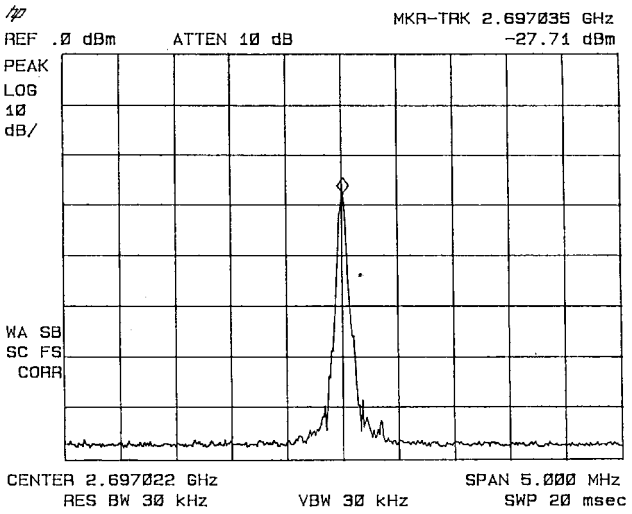

(a)

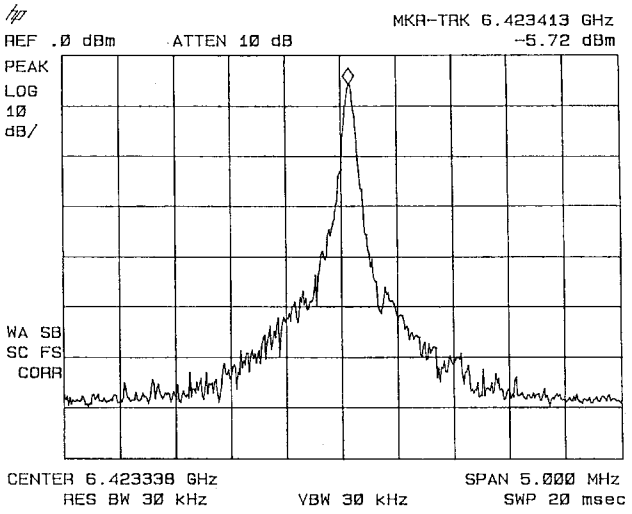

(b)

Fig. 6. Measured oscillation modes for a 6 × 6 grid backed by a high-permittivity substrate and mirror. (a) 2.7 GHz. (b) 6.4 GHz. Each mode was obtained separately at different dc bias currents: 5 mA/device for (a) and 12 mA/device for (b).

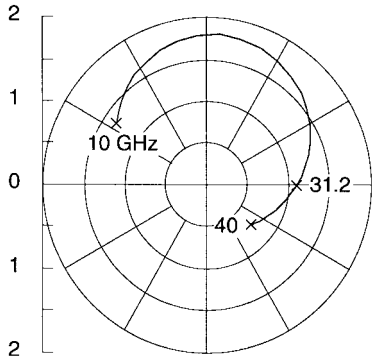

Fig. 7. Circular function for a monolithic 100-pHEMT grid oscillator. The predicted oscillation frequency is 31.2 GHz, which agrees with the measured frequency of 31.1 GHz.

equivalent circuits are shown, each corresponding to a different frequency. In both cases, the negative resistance is greater than the load resistance, thus, oscillation is possible.

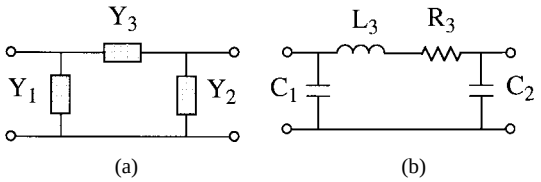

Fig. 8. (a) General lumped equivalent circuit for a two-port network, where $Y_1 = Y_{11} + Y_{12}$, $Y_2 = Y_{22} + Y_{12}$, and $Y_3 = -Y_{12}$. (b) Typical form of the equivalent circuit for a grid.

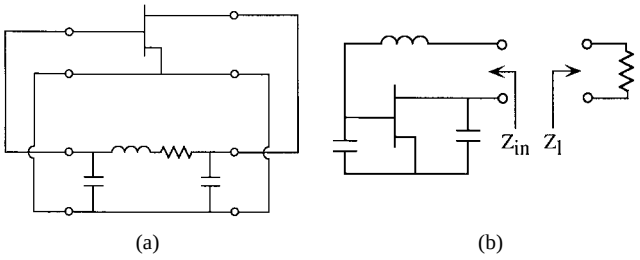

Fig. 9. (a) Transistor connected to the equivalent Π network. (b) Negative-resistance model of the grid oscillator.

III. Synthesis of the Optimum Grid Equivalent Circuit

The lumped equivalent circuit discussed above can be optimized for maximum oscillator power. The general approach is described in [10]. Briefly, the equivalent Π network, shown in Fig. 8(a), is synthesized to satisfy the oscillation condition and to set the proper feedback level and load resistance for maximum power. The embedding elements are given by [11]

$$B_1 = \frac{A_r}{A_i}(C_1 + C_3) + C_2 + C_4$$

$$B_2 = -\frac{1}{A_i}(C_1 + C_3)$$

$$B_3 = \frac{1}{|1-A|^2}\left\{(A_r - 1)\left[C_4 + \frac{A_r}{A_i}(C_1 + C_3)\right] + A_i C_1\right\}$$

$$G_3 = \frac{1}{|1-A|^2}(C_1 + A_r C_3 + A_i C_4)$$

where $Y_i = G_i + jB_i$

$$C_1 = -\mathrm{Re}(Y_{11} + AY_{12}) \quad C_3 = -\mathrm{Re}(Y_{21} + AY_{22})$$
$$C_2 = -\mathrm{Im}(Y_{11} + AY_{12}) \quad C_4 = -\mathrm{Im}(Y_{21} + AY_{22})$$

and $A = A_r + jA_i$ is the voltage gain in the feedback loop, as discussed in [10] and [12].

The design of this network is based on the large-signal Y-parameters of the active device corresponding to the point of optimum gain compression. These parameters can be found, for example, using the approximation described by Johnson [13], who showed that the large-signal effects associated with transistor saturation can be approximated by simply reducing the device's $|S_{21}|$ and assuming that all other S-parameters remain the same as their small-signal values.

The advantage of this synthesis approach is that a number of key elements are built-in. This approach: 1) satisfies the oscillation start-up condition at small-signal levels ($|C| > 1$); 2) satisfies the steady-state oscillation condition at large-signal levels ($|C| = 1\angle 0°$); 3) is designed for a specified oscillation frequency; and 4) is designed for the proper level of feedback for optimum gain compression, thus maximizing oscillator power.

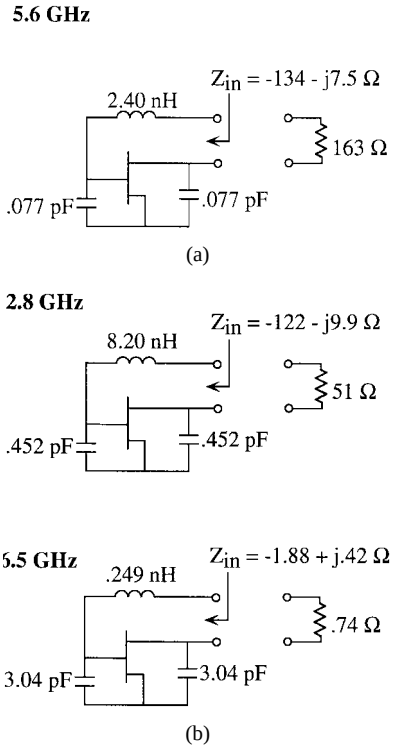

Fig. 10. Negative-resistance model for the grids associated with (a) Fig. 5(a) and (b) Fig. 5(b).

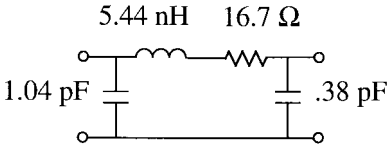

Fig. 11. Optimum lumped equivalent circuit for the HP-Avantek ATF-26836 MESFET at 3 GHz.

As an example, the optimum lumped equivalent circuit for the HP-Avantek ATF-26836 MESFET is shown in Fig. 11. Note that this design approach predicts that the optimum grid geometry for this device is not symmetric. Rather, the optimum grid should present a larger capacitance to the gate–source port of the transistor than to the drain–source port. A grid designed using this approach will be described in Section V.

IV. Benchmarking Grid-Oscillator Performance

Once the optimum embedding network has been determined for a given transistor, the associated circular function can be computed from (3) and used as a benchmark for determining whether a given grid oscillator has too little or too much feedback.

It is useful to use the concept of maximum-efficient gain [14], [15], defined as

$$G_{\mathrm{ME}} = \frac{|S_{21}/S_{12}|^2 - 1}{2(K|S_{21}/S_{12}| - 1)} \tag{4}$$

where

$$K = \frac{1 + |S_{11}S_{22} - S_{21}S_{12}|^2 - |S_{11}|^2 - |S_{22}|^2}{2|S_{12}||S_{21}|}.$$

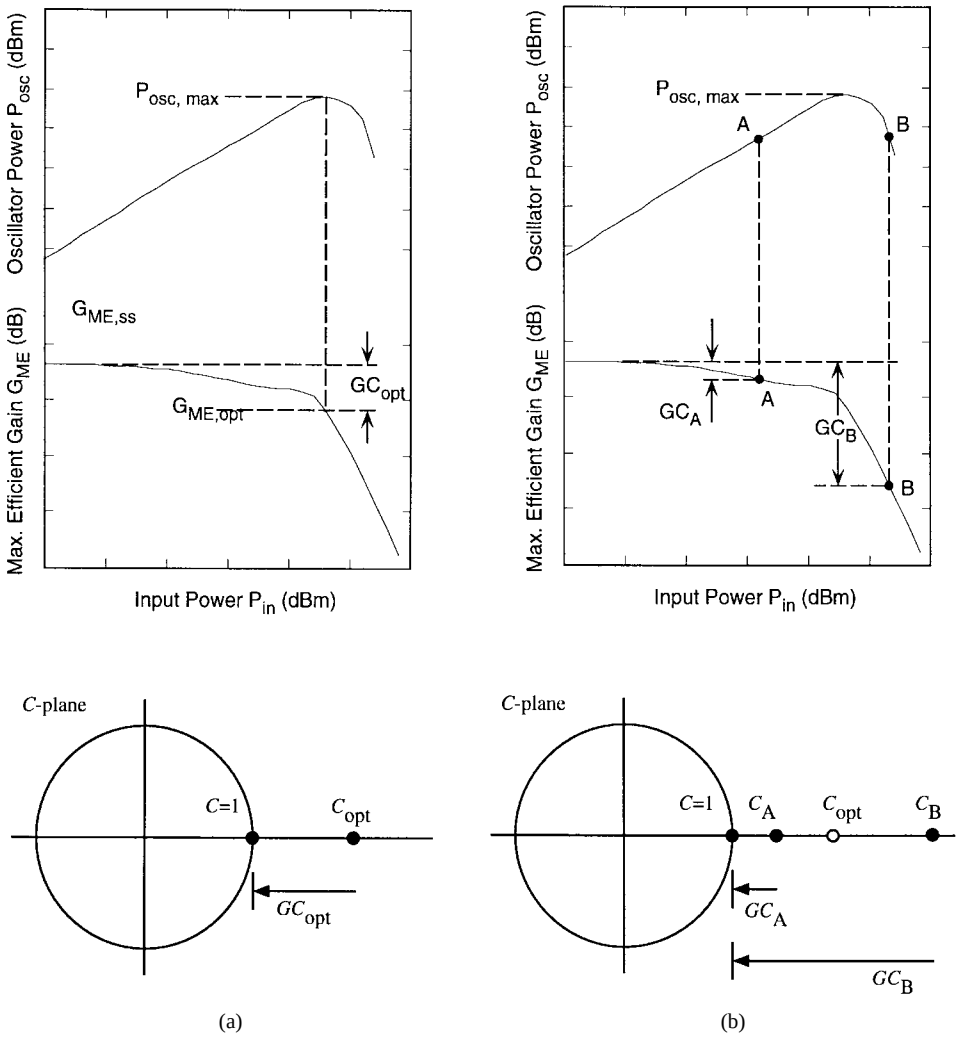

Fig. 12. Transistor saturation characteristics and circular-function plane for (a) the optimal operating point, and (b) two suboptimal operating points. $P_{\rm in}$ is the input power to the transistor, as indicated in Fig. 2(b), and $P_{\rm osc} = P_{\rm out} - P_{\rm in}$ is the radiated power.

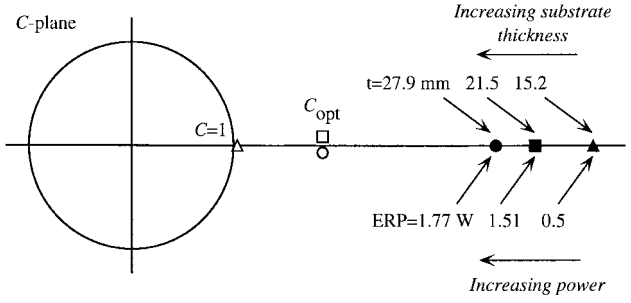

Fig. 13. Operating points corresponding to three different substrate thicknesses for a C-band pHEMT grid oscillator. The shaded symbols represent the C-functions of the grids, and the open symbols represent the C-functions of the theoretical optimum networks. The measured ERP is also shown.

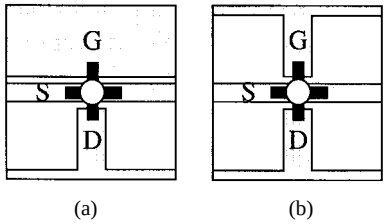

Fig. 14. Unit cell of a grid oscillator with (a) slot/dipole radiating elements and (b) dipole radiating elements. Both cells are 6-mm square and are loaded with HP-Avantek ATF-26884 MESFET's. The grids are printed on a 0.5-mm substrate (Duroid 5880, $\epsilon_r = 2.2$) and placed on a second 5-mm layer (Duroid 6010.8, $\epsilon_r = 10.8$) which is metallized on the back.

Johnson [13] showed that the large-signal value of $G_{\rm ME}$ corresponding to maximum oscillator power is

$$G_{\rm ME,opt} = \frac{G_{\rm ME,ss} - 1}{\ln G_{\rm ME,ss}} \tag{5}$$

where $G_{\rm ME,ss}$ is the value of (4) computed using the small-signal transistor S-parameters. The gain compression corresponding to the optimum operating point is then

$$GC_{\rm opt} = G_{\rm ME,ss} - G_{\rm ME,opt}. \tag{6}$$

Since the S-parameters are frequency-dependent, the circular function is actually a locus of points, but the particular point of interest for this discussion is the frequency at which $\angle C = 0°$. Two cases are shown in Fig. 12.

In the optimum case, the small-signal value of C should be displaced from its large-signal steady-state value (i.e., $1\angle\ 0°$) by an amount corresponding to $GC_{\rm opt}$ [see Fig. 12(a)]. Since this value of C corresponds to the optimum case, it is referred to as $C_{\rm opt}$. There are two operating points shown in Fig. 12(b) that represent suboptimal performance. Both cases

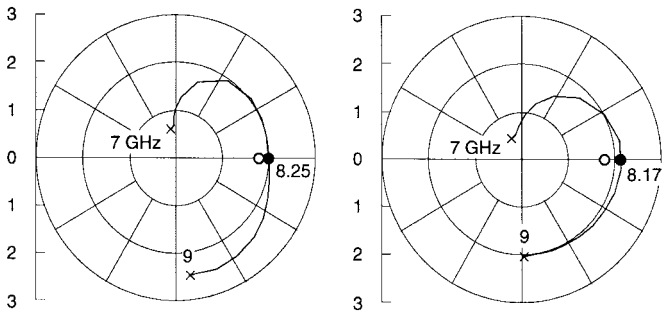

(a) (b)

Fig. 15. C-functions for the (a) slot/dipole- and (b) dipole–grid oscillators. The shaded symbols represent the C-functions of the grids, and the open symbols represent the C-functions of the theoretical optimum networks.

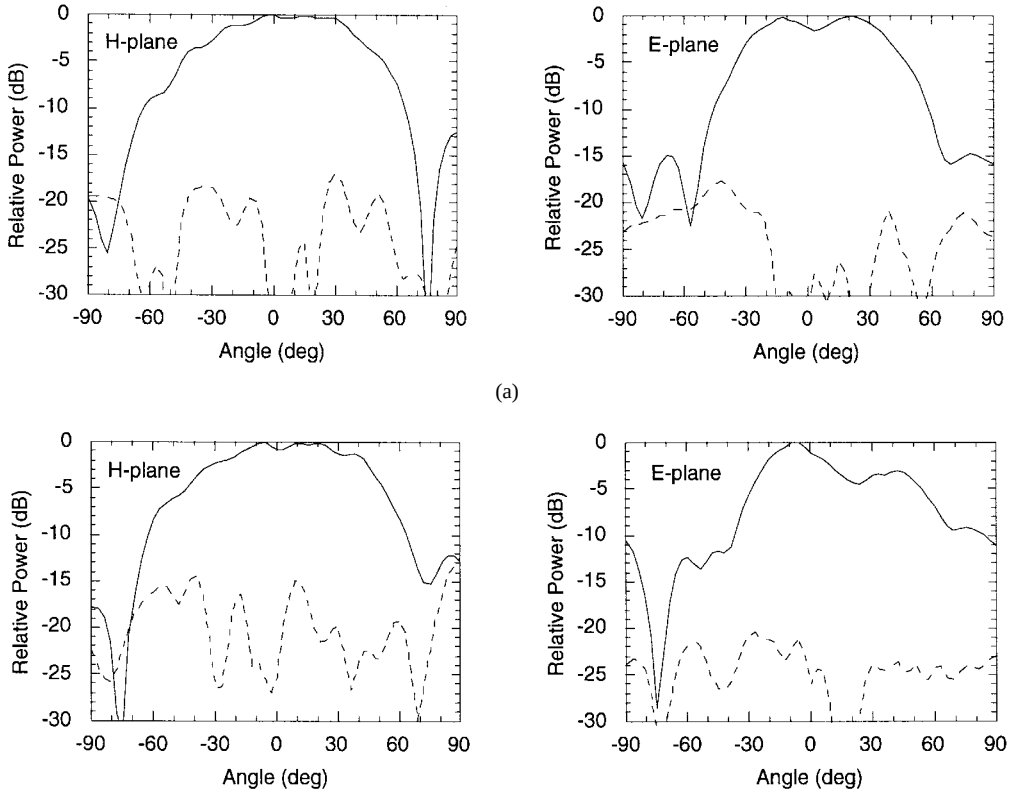

(a)

(b)

Fig. 16. Measured H- and E-plane patterns of the (a) slot/dipole- and (b) dipole–grid oscillators of Fig. 14. Solid lines represent the copolarization and dashed lines represent the cross polarization.

have less than the maximum available oscillator power, but for different reasons: point A suffers from gain compression that is too low $(GC_A < GC_{\rm opt})$, while point B suffers from gain compression that is too high $(GC_A > GC_{\rm opt})$. For point A, the transistor operates in the near-linear regime since the circular function requires only a small amount of gain compression to reach steady state. For point B, the transistor is heavily compressed since the feedback level is too high.

There are several disadvantages of operating at point B. In this regime, the oscillator power drops off more sharply, so it is more sensitive to design variations in the feedback network. An oscillator operating in the nonlinear regime is also more likely to have higher harmonic content. For a MESFET, point B is also associated with high input power at the gate, which could cause the Schottky gate diode to be driven into forward-bias; this could result in a large current density in the gate metallization, which can lead to degraded device reliability.

Most grid oscillators demonstrated to date have had too much feedback [5]. The design of an optimized grid must, therefore, include a feedback-reduction mechanism to move the circular function toward $C_{\rm opt}$.

To illustrate, consider a 5×5 pHEMT grid oscillator with varying substrate thickness. Three C-functions, corresponding to different thicknesses of Emerson and Cuming Stycast HiK $(\epsilon_r = 10)$, are shown in Fig. 13.

Since the oscillation frequency is different for each case (see Table I), three different optimum embedding circuits can

TABLE I
C-BAND pHEMT GRID OSCILLATOR

Substrate Thickness (mm)	Osc. Freq. (GHz) Sim.	Meas.	% Err.	Meas. ERP (W)	Harmonics(dBc) 2^{nd}	3^{rd}
15.2	6.4	6.07	5	0.50	-28	-42
21.5	4.6	4.86	5	1.51	-25	-45
27.9	5.1	5.32	4	1.77	-31	-45

TABLE II
X-BAND MESFET GRID OSCILLATOR

Unit-Cell Geometry	Osc. Freq. (GHz) Sim.	Meas.	% Error	Meas. ERP (W) V_{ds} =3 V	V_{ds}=4 V
Slot/Dipole	8.3	8.57	3	0.31	0.49
Dipole	8.1	8.35	3	0.19	0.31

be derived. For the three different frequencies, C_{opt} is plotted in Fig. 13.

Since $|C| > |C_{\text{opt}}|$ for all three cases, we immediately conclude that the grids have excessive feedback. Moreover, the grid with the thinnest substrate is the most compressed, and should have the least power. The experimental results in Table I support this. The existence of harmonics also supports the view that these oscillators are over-compressed.

V. OPTIMIZING GRID PERFORMANCE

The example above demonstrates how the feedback level can be controlled by varying the substrate thickness. Another way of controlling the feedback is to alter the unit-cell geometry in some way. Hacker *et al*. [5] used a meandered gate lead to control the compression level in a gate–feedback grid. For a source–feedback grid, the feedback can be controlled by using an asymmetric unit cell [see Fig. 14(a)], as suggested by the asymmetric optimum circuit of Fig. 11. As before, the drain is connected to a short dipole radiating element. However, the width of the radiating element connected to the gate is extended across the full width of the unit cell, resulting in a slot, rather than dipole radiator. By adjusting the dimensions of this slot, the amount of feedback to the gate and, hence, the compression level, can be controlled to some extent.

To demonstrate, two 4×4 X-band grid oscillators were fabricated with the metallization patterns shown in Fig. 14. Both grids have the same unit-cell dimensions, substrate, and mirror spacing. The simulated C-functions are shown in Fig. 15. At the same dc bias level, the slot/dipole–grid oscillator demonstrated up to 58% more ERP than the dipole–grid oscillator (Table II). While both grids are slightly overcompressed, they are not as compressed as the pHEMT grids discussed earlier. No harmonics were observed for either grid.

Fig. 16 shows the measured radiation patterns. Based on an estimate of the directivity from these patterns, the highest conversion efficiency for the slot/dipole grid was 21%, while that of the dipole grid was approximately 10%.

VI. CONCLUSION

Five different grid oscillators, covering S through Ka bands, were designed using the unit-cell approximation and analyzed using the circular-function method. In all cases, the predicted oscillation frequency was within 5% of the measurement. An analytical method was presented for determining the embedding circuit for a grid oscillator that results in maximum oscillator power. Experimental results were correlated to theory, demonstrating how the substrate thickness and metallization pattern could be varied to optimize the feedback level and increase the ERP.

REFERENCES

[1] Z. B. Popović, R. M. Weikle II, M. Kim, and D. B. Rutledge, "A 100-MESFET planar grid oscillator," *IEEE Trans. Microwave Theory Tech.*, vol. 39, pp. 193–200, Feb. 1991.

[2] R. M. Weikle II, M. Kim, J. B. Hacker, M. P. De Lisio, Z. B. Popović, and D. B. Rutledge, "Transistor oscillator and amplifier grids," *Proc. IEEE*, vol. 80, pp. 1800–1809, Nov. 1992.

[3] Z. B. Popović, W. A. Shiroma, and R. M. Weikle II, "Grid oscillators," in *Active and Quasi-Optical Arrays for Solid-State Power Combining*, R. A. York and Z. B. Popović, Eds. New York: Wiley, 1997, ch. 8.

[4] A. P. S. Khanna and J. Obregon, "Microwave oscillator analysis," *IEEE Trans. Microwave Theory Tech.*, vol. MTT-29, pp. 606–607, June 1981.

[5] J. B. Hacker, M. P. De Lisio, M. Kim, C.-M. Liu, S.-J. Li, S. W. Wedge, and D. B. Rutledge, "A 10-W X-band grid oscillator," in *1994 IEEE MTT-S Int. Microwave Symp. Dig.*, San Diego, CA, May 1994, pp. 823–826.

[6] R. D. Martinez and R. C. Compton, "A general approach for the s-parameter design of oscillators with 1 and 2-port active devices," *IEEE Trans. Microwave Theory Tech.*, vol. 40, pp. 569–574, Mar. 1992.

[7] S. C. Bundy and Z. B. Popović, "A generalized analysis for grid oscillator design," *IEEE Trans. Microwave Theory Tech.*, vol. 42, pp. 2486–2491, Dec. 1994.

[8] S. J. Mason, "Feedback theory—Further properties of signal flow graphs," *Proc. IRE*, vol. 44, pp. 920–926, July 1956.

[9] J. Geddes, personal communication, Mar. 1995.

[10] M. Vehovec, L. Houselander, and R. Spence, "On oscillator design for maximum power," *IEEE Trans. Circuit Theory*, vol. CT-15, pp. 281–283, Sept. 1968.

[11] G. D. Vendelin, A. M. Pavio, and U. L. Rohde, *Microwave Circuit Design Using Linear and Nonlinear Techniques*. New York: Wiley, 1990, p. 450.

[12] B. K. Kormanyos and G. M. Rebeiz, "Oscillator design for maximum added power," *IEEE Microwave Guided Wave Lett.*, vol. 4, pp. 205–207, June 1994.

[13] K. M. Johnson, "Large signal GaAs MESFET oscillator design," *IEEE Trans. Microwave Theory Tech.*, vol. MTT-27, pp. 217–227, Mar. 1979.

[14] K. L. Kotzebue, "Maximally efficient gain: A figure of merit for linear active 2-ports," *Electron. Lett.*, vol. 12, pp. 490–491, Sept. 1976.

[15] ——, "Microwave amplifier design with potentially unstable FET's," *IEEE Trans. Microwave Theory Tech.*, vol. MTT-27, pp. 1–3, Jan. 1979.

Wayne A. Shiroma (S'85–M'96) was born in Los Angeles, CA, on February 4, 1963. He received the B.S. degree from the University of Hawaii at Manoa, in 1986, the M.Eng. degree from Cornell University, Ithaca, NY, in 1987, and the Ph.D. degree from the University of Colorado at Boulder, in 1996, all in electrical engineering.

In 1996, he joined the University of Hawaii at Manoa, as an Assistant Professor of electrical engineering. He has also served as a Member of the Technical Staff at Hughes Space and Communications, El Segundo, CA, developing solid-state power amplifiers for satellite communications. His research interests include microwave, millimeter-wave, and quasi-optical electronics.

Zoya Basta Popović (S'86–M'90), for a photograph and biography, see this issue, p. 2174.